Reductive cleavage of the O–O bond in multicopper oxidases: a QM/MM and QM study†

Martin Srnec,[a] Ulf Ryde[b] and Lubomír Rulíšek*[a]

Received 19th March 2010, Accepted 28th April 2010
DOI: 10.1039/c004476h

The key step in the reaction mechanism of multicopper oxidases (MCOs)—the cleavage of the O–O bond in O_2—has been investigated using combined quantum mechanical and molecular mechanical (QM/MM) methods. This process represents a reaction pathway from the peroxy intermediate after it accepts one electron from the nearby type-1 Cu site to the experimentally-observed native intermediate, which is the only fully oxidised catalytically relevant state in MCOs. Scans of the QM(DFT)/MM potential energy surface have allowed us to obtain estimates of the activation energies. Furthermore, vacuum calculations on a smaller model of the active site have allowed us to estimate the entropy contributions to the barrier height and to obtain further insight into the reaction by comparing the small cluster model with the QM/MM model, which includes the entire protein. Owing to the complicated electronic structure of these low-spin exchange coupled systems, multireference quantum chemical calculations at the complete-active space second-order perturbation theory (CASPT2) were used in an attempt to benchmark the barrier heights obtained at the DFT(B3LYP) level. Our best estimate of the activation barrier is $\Delta G = 60$–65 kJ mol^{-1}, in good agreement with the experimental barrier of $\sim$55 kJ mol^{-1}, which can be inferred from the experimental rate constant of $k > 350$ s^{-1}. It has also been shown that the reaction involves protonation of the O_2 moiety before bond cleavage. The proton likely comes from a nearby carboxylate residue which was recently suggested by the experiments.

1 Introduction

In the last two decades, quantum chemical (QM) and combined quantum and molecular mechanical (QM/MM) calculations have proved to be very useful tools in elucidating the reaction mechanisms of metalloproteins.[1,2,3,4,5,6,7] Theoretical modelling can, in principle, map the correspondence between conformational space and the energy landscape, and characterise the crucial points along the reaction coordinate, most notably the transition states (TSs).[8] However, there are two strict prerequisites to the provision of quantitatively correct answers and unambiguous conclusions: the methods must be accurate enough and the models must contain

[a]*Gilead Sciences & IOCB Research Center, Institute of Organic Chemistry and Biochemistry, Academy of Sciences of the Czech Republic, Flemingovo nám. 2, 166 10 Praha 6, Czech Republic. E-mail: rulisek@uochb.cas.cz; Fax: +420 220 578; Tel: +420 220 183 263*
[b]*Department of Theoretical Chemistry, Lund University, Chemical Center, P.O. Box 124, S–221 00 Lund, Sweden. E-mail: Ulf.Ryde@teokem.lu.se*

† Electronic supplementary information (ESI) available: Protein coordinates and the point charges on all the atoms in the MM region (in PDB format) and the equilibrium geometries of the quantum region for all of the studied structures. See DOI: 10.1039/c004476h

as few approximations as possible. It is a non-trivial task to meet both of these conditions, because it is not clear, for example, whether a large cluster model of the enzyme active site can yield correct answers[3,9] or whether one has to resort to a QM/MM modelling, which includes the whole protein molecule.[1]

We consider multicopper oxidases (MCOs) to be an excellent class of compounds for addressing this question. MCOs are enzymes that couple four one-electron oxidations of a substrate with a four-electron reduction of molecular oxygen to water:[10,11]

$$O_2 + 4e^- + 4H^+ \rightarrow 2H_2O \quad (1)$$

This reaction takes place at a trinuclear copper cluster (TNC), whereas the substrate is oxidised at a type-1 copper site (Cu-T1), which is ~13 Å away from the TNC and is linked to it *via* a bifurcated $(Cu\text{-}TNC)_2$-$(His)_2$-Cys-Cu-T1 link. The link is assumed to provide the electron-transfer (ET) pathway between the two sites. The key aspects of the MCO reaction mechanism have been revealed by combining spectroscopic[12,13,14] and structural[15,16] information with the QM/MM calculations,[17] mostly for the prototypical enzyme of the MCO family—laccase.[18,19] The QM/MM calculations were further supported by multireference calculations of the MCO spectroscopic properties[20] and combined extended X-ray absorption fine-structure EXAFS/QM/MM calculations.[21] This has led to the consensus reaction mechanism depicted in Fig. 1.

The reaction starts with the fully reduced form of the enzyme, presumably with a water molecule weakly coordinated to the type-2 copper (Cu-T2) ion and no bridging moiety between the two type-3 copper (Cu-T3) ions.[17,22] The incoming dioxygen is immediately reduced, yielding a peroxide-level intermediate (**PI**),[12] with a peroxide ion bound in the centre of the TNC. The reaction is completed by the uptake of one electron from the Cu-T1 site (resulting in an activated peroxy intermediate **NI′**) to yield the native intermediate (**NI**),[14] a spectroscopically characterised, catalytically relevant, fully oxidised form of the enzyme. The **NI** has one μ_3-oxo ligand bridging all three copper ions and a μ_2-hydroxo ligand bridging the two

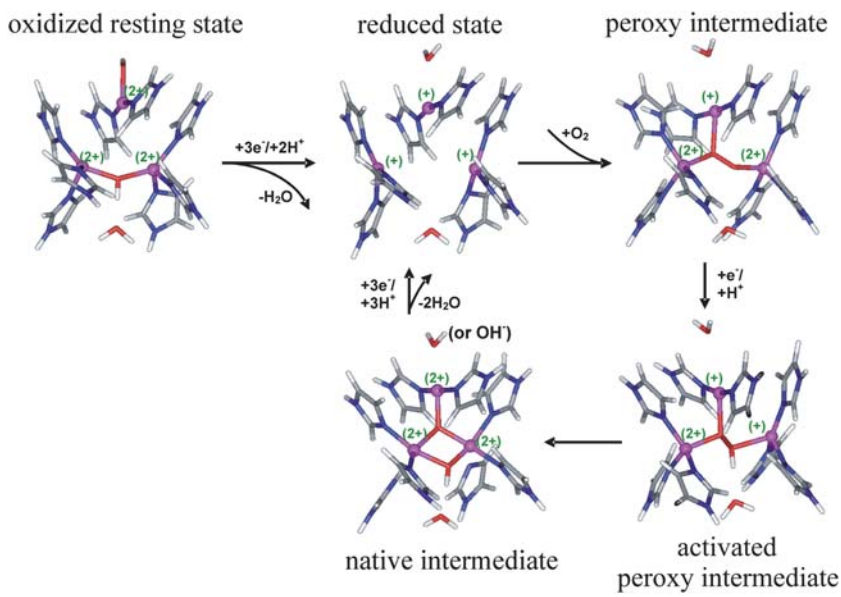

Fig. 1 The consensus MCO reaction mechanism.[17]

Cu-T3 ions.[17,20] It is suggested that the resting oxidised state is not involved under catalytic turnover conditions[14] since its transformation into the fully reduced form is too slow when compared to the overall reaction rate. The mechanism in the form depicted in Fig. 1 was first proposed by Rulíšek *et al.*,[17] later confirmed experimentally by Yoon *et al.*,[23] and has been thoroughly reviewed recently.[22]

The energetics of the O_2-cleavage reaction step (**NI′** → **NI** pathway) have recently been studied in detail by Yoon and Solomon[25] using a cluster model (*i.e.* a truncated system representing an active site with many atoms at the edge of the QM system fixed at their crystallographic positions), during which an activation barrier of ~20 kJ mol^{-1} was found, indicating a facile reaction. However, there are three issues related to the MCO reaction coordinate presented worth addressing with QM/MM calculations that consider the whole protein. First, in the cluster model, one has to fix atoms at the borderline of the QM system, an approximation that is automatically taken care of (avoided) in QM/MM calculations. For example, the calculated reaction energy of the O_2-cleavage in MCO using a cluster model ($\Delta E = -213$ kJ mol^{-1})[25] originates from the high exothermicity (ΔH) of the uncatalysed $H_2 + H_2O_2 \rightarrow 2H_2O$ reaction ($\Delta H = -347$ kJ mol^{-1}),[26] and one may expect this large exothermicity to be even more buffered by the protein. In our opinion, this large thermodynamic driving force in the MCO cluster model may imply an artificial lowering of the activation barrier following the Hammond postulate (see Fig. 2).[27]

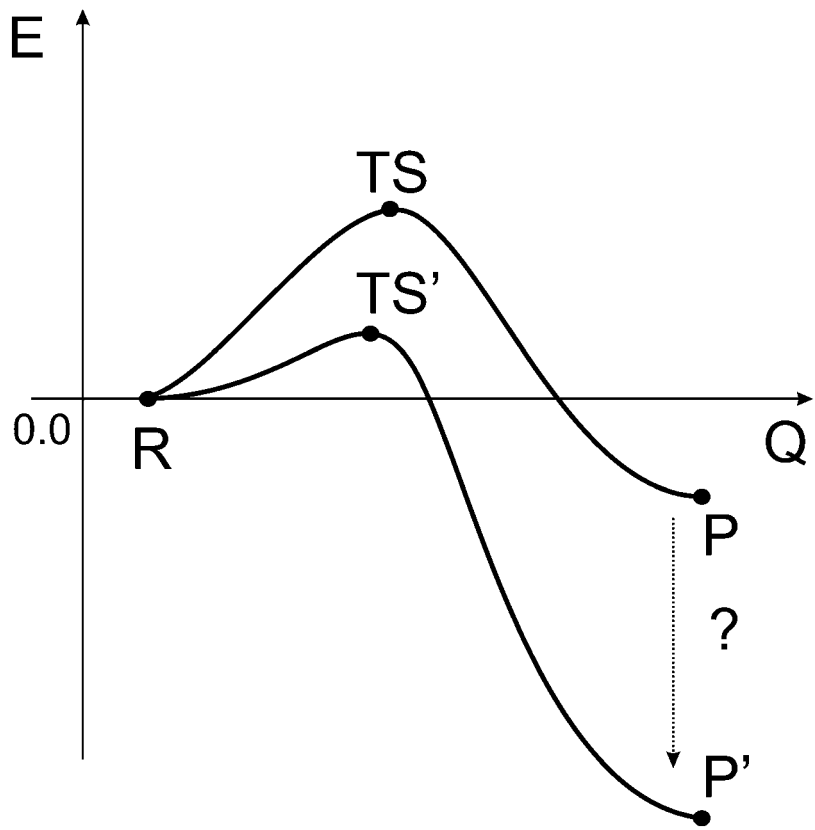

Fig. 2 The overstabilisation of the product state may lead to an artificial lowering of the activation barrier.[27] A similar effect has recently been shown in the model reactions of boron compounds.[48]

The accuracy of the cluster-model approximation is even more relevant for MCOs (in comparison with other metalloproteins) since the TNC in many of its oxidation and protonation states is inherently unstable *in vacuo*.[17] Its stability is maintained in the protein by the presence of neutralising carboxylate residues that are conserved in the MCO family[17] and four His–X–His motifs (with His being ligands of copper ions in TNC) that are sewing the TNC site together. This raises the second issue, namely what size of a model system is needed in QM calculations? Only after explicitly including carboxylate moieties into the calculations were the correct structures of the peroxy intermediate obtained in the QM calculations.[25] Finally, despite DFT methods being widely used in the calculations of bioinorganic systems and most often providing results of satisfactory accuracy, one may attempt to benchmark them carefully, especially for systems with complicated electronic structures like the exchange-coupled copper ions in oxidised TNC.

The aim of this work is to perform a careful investigation of the O_2 cleavage reaction in the MCOs—by QM/MM methods, performing a structural and energetic characterisation of the activation barriers for the various protonation states of the active site, complementing the *in vacuo* data obtained by Yoon and Solomon.[25] The QM/MM description quite naturally includes both the electrostatic and sterical effects of the protein environment and can in principle yield correct energetics along the reaction pathway. Moreover, we have also attempted to estimate the entropic contributions acquired from a cluster model and to benchmark the DFT methods by high-level multireference *ab initio* calculations. This can complete our understanding of the reaction mechanism of MCOs at the theoretical level, which includes the full protein environment.

2 Computational details

2.1 Combined quantum mechanical and molecular mechanical calculations

All of the QM/MM calculations were carried out using the ComQum program.[28,29] It is a combination of Turbomole 5.7[30] for the QM part with AMBER 8[31] and the Cornell *et al.* force field[32] for the MM part. In this approach, the protein and solvent are split into three subsystems; the QM region (System 1) contains the most interesting atoms and is relaxed by the QM/MM forces. System 2 consists of all the residues within 6 Å of any atom in System 1 and is relaxed by a full MM minimisation in each step of the QM/MM geometry optimisation. Finally, System 3 contains the remaining part of the protein and surrounding solvent molecules, and is kept fixed at the original coordinates. In the quantum chemical calculations, the QM system is represented by a wave function, whereas all of the other atoms are represented by an array of partial point charges, one for each atom, taken from Amber libraries. The total QM/MM energy is then calculated as:

$$E_{\mathrm{QM/MM}} = E_{\mathrm{QM1}} + E_{\mathrm{MM123}} - E_{\mathrm{MM1}} \quad (2)$$

where E_{QM1} is the QM energy of System 1, including a point-charge model of the surroundings (electric embedding), E_{MM123} is the MM energy of the full system but ignoring the electrostatic interactions between System 1 and the other systems (to avoid double-counting), and E_{MM1} is the MM energy of System 1. The computational protocol is essentially identical to the one used previously in the characterisation of the key intermediates in MCO.[17] In ref. 17, further details of the QM/MM procedure can be found.

2.2 Protein setup

All of the QM/MM calculations are based on the 1.4 Å structure of CueO (PDB code 1KV7).[33] This structure was selected because it had the best resolution of all the MCO structures published at the beginning of this investigation. In addition, it is

a monomer and lacks glycosylated surface residues, which are common in eukaryotic proteins. Hydrogen atoms were added to the crystal structure and the total system was solvated in a sphere of water molecules with a radius of 38 Å. The positions of the hydrogen atoms and solvent water molecules were then optimised by a 90 ps simulated-annealing calculation with molecular dynamics followed by a conjugate-gradient energy minimisation of their positions. We assumed the normal protonation state at pH 7 for all of the amino acids, except for the copper-bound Cys residue, which was assumed to be deprotonated. For the His residues, the protonation status was decided based on a detailed study of the hydrogen-bond network around the residue and the solvent accessibility. Thus, His-71, 111, 113, 393, 395, 446 and 448 were assumed to be protonated on the $N^{\delta 1}$ atom, His-73, 390, and 452 on the $N^{\varepsilon 2}$ atom, and the other eight His residues on both of these atoms. The space created by a disordered loop, missing in the CueO crystal structure (residues 380–402; more than 22 Å from the trinuclear copper cluster), was filled by water molecules. System 1 (the QM system) consisted of the following residues: the three copper ions of TNC and their eight His ligands, O_2 or water derived ligands of the three copper ions, two carboxylate groups close to the TNC (Asp-82 and Glu-453) as well as three water molecules bridging between them with the TNC. The size of the quantum system was approximately 105 atoms (*cf*. Fig. 5).

2.3 Quantum chemical calculations

All of the quantum chemical calculations were performed at the density functional theory (DFT) level. The geometry optimisations were carried out using the Perdew–Burke–Ernzerhof (PBE) functional.[34] The DFT/PBE calculations were expedited by expanding the Coulomb integrals in an auxiliary basis set (the resolution-of-identity approximation, RI-J).[35,36] All of the geometry optimisations were performed using the 6-31G(d) basis set for all of the atoms,[37] except for copper, for which we used the DZP basis sets of Schäfer *et al.*[38] (referred to as the DZP basis sets). More accurate energies were then estimated by single-point calculations using a larger basis set, namely the def2-TZVP[39] and Becke's three-parameter hybrid functional (B3LYP).[40] The structures were optimised until the change in energy between two iterations was below 0.026 J mol^{-1} (10^{-8} a.u.) and the maximum norm of the internal gradients was below 5.0 kJ mol^{-1} $Å^{-1}$ (10^{-3} a.u). The zero-point energies, thermal corrections to the Gibbs free energy and entropic terms were obtained from a normal-mode analysis on small *in vacuo* models (unlike System 1 in the QM/MM model, these models do not contain carboxylate groups and two additional waters) of the active site (*i.e.* ~85 atoms) using the same method and software as was used for the geometry optimisations. They were calculated at 298.15 K and under 1 atm pressure, using an

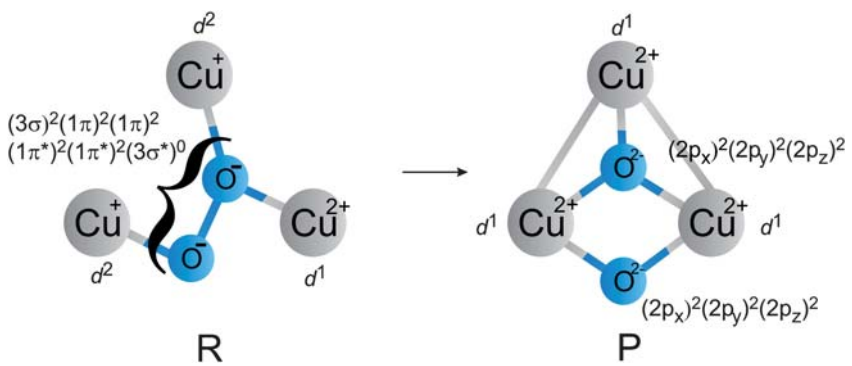

Fig. 3 A schematic description of a minimum active space, including the most important orbitals involved in the catalytic O–O bond cleavage by MCOs.

ideal-gas, rigid-rotor harmonic-oscillator approximation.[41] All of the calculations were carried out for the antiferromagnetically coupled $S = 1/2$ potential energy surface, which is a ground state for both reactants and products. In DFT, it rather means a $M_S = 1/2$ state, since we use spin-flipped Kohn–Sham determinants starting from unrestricted high-spin configurations.

The complete active space self-consistent field (CASSCF),[42] and complete active space second-order perturbation theory (CASPT2)[43] calculations were carried out using the MOLCAS 7.0 program.[44] The active space comprises fifteen electrons distributed in nine orbitals as schematically shown in Fig. 3. In all of the state-averaged CASSCF calculations (over the two near-degenerate doublet states), a level shift of 5.0 a.u. was used to improve the convergence of the multireference wave function. In the CASPT2 calculations, an imaginary level shift of 0.2 a.u. was used to eliminate intruder states.[45] The ANO-S basis set[46] with the following contractions was used: Cu [5s4p2d1f], C, O, N [3s2p] and H [2s].

2.4 Scans of the QM/MM potential energy surface. The approximate transition states in QM/MM models

Due to the lack of QM/MM analytical second derivatives in ComQum, two different strategies for mapping the QM/MM potential energy surface and searching for the transition-state structures along the reaction coordinates were adopted in this study. The first (and more conventional) approach (*cf.* Fig. 4A) starts from the reactant structure (**NI′**) and scans the elongation of the O–O bond. Once the product structure is reached, a scan is conducted in the reverse direction. These back-and-forth scans should converge to a potential-energy profile independent of the starting (*i.e.* reactant or product) structure. The disadvantage of such a procedure is the relatively slow convergence to a stable pathway. Alternatively, another strategy in the search for the QM/MM TS was adopted (*cf.* Fig. 4B), which can be described as follows: (i) the TS of the gas-phase cluster (using an *in vacuo* QM model) with one imaginary frequency is found; (ii) a QM/MM optimisation of the whole protein is carried out with the key atoms in the quantum regions (System 1) restrained to the TS obtained in the QM model (*i.e.* the distances between the Cu1, Cu2, Cu3, $O1_{peroxo}$ and $O2_{peroxo}$ atoms); (iii) the QM/MM optimisation is repeated but now only with one restrained distance between the two oxygen atoms in the peroxo species ($d_{O\text{–}O}$). Starting from this structure (denoted as $\mathbf{S_i}$), two nearby structures ($\mathbf{S_{i-1}}$, $\mathbf{S_{i+1}}$) with restrained distances $d_{O\text{–}O}(\mathbf{S_{i-1}}) = d_{O\text{–}O}(\mathbf{S_i}) - 0.05$ Å and $d_{O\text{–}O}(\mathbf{S_{i+1}}) = d_{O\text{–}O}(\mathbf{S_i}) + 0.05$ Å, respectively, are optimised. If $E(\mathbf{S_{i-1}}) < E(\mathbf{S_i}) > E(\mathbf{S_{i+1}})$, then the structure $\mathbf{S_i}$ is considered to be the TS in the QM/MM model, otherwise the $\mathbf{S_{i-2}}$, $\mathbf{S_{i+2}}$ structures are taken into account. This procedure is repeated until the maximum on the PES is found ($\mathbf{S_{TS}}$), which corresponds to the approximate QM/MM TS. The nature of the TS can be simply verified by the optimisation of the $\mathbf{S_{TS-1}}$ and $\mathbf{S_{TS+1}}$ structures converging to the reactants and products, respectively.

3 Results and discussion

3.1 The QM/MM reaction coordinates of O_2 cleavage in MCOs

Six alternatives for the reaction pathways corresponding to the cleavage of the O–O bond in MCOs were studied. These included two protonation states of the peroxide moiety (O_2^{2-} and O_2H^-), and three possibilities concerning the Cu-T2 ligand (H_2O, OH^-, no ligand). Two representative pathways (with H_2O as the Cu-T2 ligand) are depicted in Fig. 5. We postulated[17] the existence of a transient species—activated by a peroxy intermediate (**NI′**)—structural analogue of the **PI** with the Cu-T1 site oxidised and one more electron available in TNC (denoted as **PI + e** by Yoon and Solomon[25]). It is, therefore, the last chemically distinct species prior to the cleavage of the O–O bond. The product of the reaction is the experimentally characterised **NI**

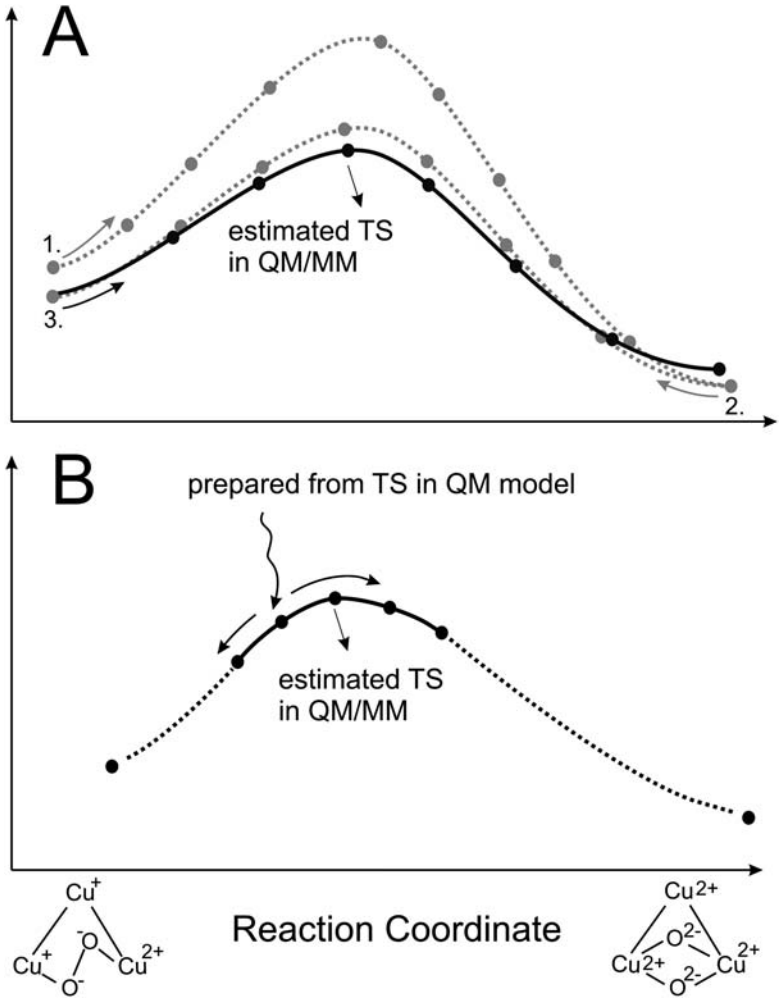

Fig. 4 The two different strategies to estimate the transition state (TS) in the QM/MM model. A. The O–O distance is scanned to and back in the QM/MM calculations until the stable coordinate is found. B. The transition state is obtained in the QM calculations and is projected into the QM/MM calculations by fixing few distances to their values in the QM calculation.

in the μ_3-oxo binding mode of O^{2-}, which has been shown to be energetically more favourable than three μ_2-hydroxo bridges on all of the three Cu–Cu sides.[17]

The calculated activation barriers and reaction energies are listed in Tables 1 and 2, respectively. These include the total QM/MM energies and the non-electrostatic (steric) MM contribution to the total QM/MM energy, E_{MM} term ($E_{MM} = E_{MM123} - E_{MM1}$). The third term in eqn (1), the quantum-mechanical energy with the point charges included in the one-electron Hamiltonian (the QM energy, including the electrostatic stabilisation of the quantum system by the surrounding protein), E_{QM1}, has not been included, since it can be trivially calculated as the difference of the $E_{QM/MM}$ and E_{MM} terms. For a comparison, the single-point energies at the optimised QM/MM geometries of System 1 for the same reaction step *in vacuo* are also given ($E_{QM/vac}$).

It can be seen that all of the activation barriers are quite close to each other with $\Delta E^{\neq} = 59-81$ kJ mol^{-1} ($\Delta G^{\neq} = 63-79$ kJ mol^{-1}). These values are also close to the

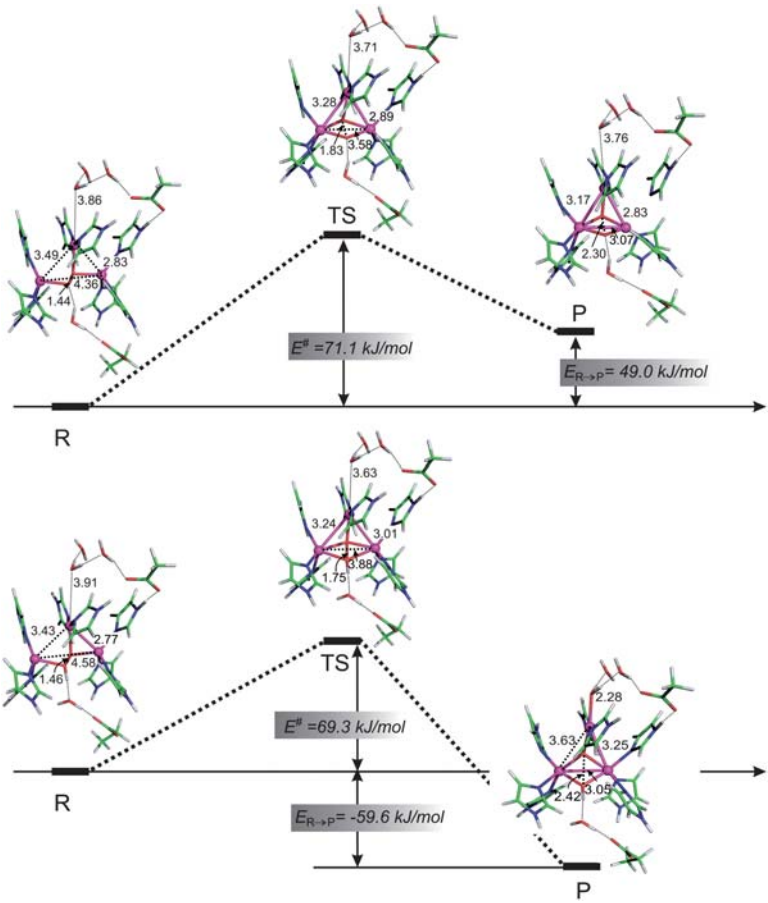

Fig. 5 The QM/MM optimised structures for two of the six studied **NI′** → **NI** reaction pathways (O_2 cleavage in MCOs), starting from the two states with the Cu-T2 ligand H_2O and with either an O_2^{2-} (top) or HO_2^- (bottom) in the centre of the TNC cluster. All of the distances are in Å.

value of $\Delta G^{\neq}_{exp} < 55$ kJ mol^{-1}, which can be deduced from the rate of $k_{cat} > 350$ s^{-1} (from ref. 13) using Eyring's equation. The Cu-T2 ligand in the **PI** is normally assumed to be an H_2O and the central peroxide in the O_2^{2-} protonation state.[12,17] Our preliminary calculations indicate that reducing **PI** to **NI′** would significantly shift the pK_a value of the central O_2^{2-} ligand from 0 to 11, and we therefore expect that a reduction of the T23 site is immediately followed by a protonation of O_2^{2-}. The proton is likely taken from one of the two carboxylate moieties that are part of our QM/MM system (*cf.* Fig. 5). This observation (glutamate near the T3 copper acts as the proton donor) has been recently inferred from experiments on the Fet3p MCO.[47]

The fact that the protonation of O_2^{2-} may precede the O–O bond cleavage can be supported by a comparison of two alternative pathways: **NI′**{OH^-,—,O_2H^-} → **NI**{OH^-,OH^-,O^{2-}:C} and **NI′**{H_2O,—,O_2^{2-}} → **NI**{H_2O,O^{2-},O^{2-}:C}. [Here and below, we have introduced the notation used in Ref. 17, where in **X**{A,B,L:P} A denotes the Cu-T2 ligand; B, if present, the Cu-T3/Cu-T3′ μ_2-bridging moiety; L the ligand in the centre of the $(Cu)_3$ triangle; and P specifies its position (*e.g.* P = C denotes μ_3- coordination)]. Although the calculated energy difference between the corresponding **NI′** states is very similar (within ±4 kJ mol^{-1} for the QM/MM

Table 1 The calculated QM/MM activation barriers ($\Delta E^{\neq}_{QM/MM}$) for the O–O bond cleavage in CueO along with the individual contributions[a]

Cu-T2 ligand[b]	Central ligand	Charge of System 1	$\Delta E^{\neq}_{QM/vac}$[c]	$\Delta E^{\neq}_{MM}$[d]	$\Delta E^{\neq}_{QM/MM}$	$\Delta G^{\neq}_{QM/MM}$[e]
H_2O	O_2H^-	+1	88.7	−3.2	69.3	66.8
			89.8	−2.5	69.5	67.0
OH^-	O_2H^-	0	—	—	—	—
			38.9	6.2	59.0	—
—	O_2H^-	+1	81.7	5.0	80.6	79.4
			82.1	−0.9	75.1	73.7
H_2O	O_2^{2-}	0	64.1	0.8	71.1	72.4
			53.4	1.0	70.0	71.3
OH^-	O_2^{2-}	−1	84.6	−13.3	68.1	73.7
			61.6	5.4	64.6	70.2
—	O_2^{2-}	0	66.8	−6.4	73.9	78.4
			67.5	1.6	73.0	77.5

[a] The geometries were optimised at the QM(RI-PBE/DZP)/MM level, whereas the single-point energies were recalculated at the QM(B3LYP/def2-TZVP)/MM level. The total energies of the reactants (**NI′**) are set to zero. All of the values are in kJ mol^{-1}. [b] For each system, two rows of numbers have been introduced, the first of which corresponds to the results obtained from Scan B and the second to the results obtained from Scan A (both procedures are depicted in Fig. 4 and described in Section 2.4). [c] The *in vacuo* QM energy change of System 1. [d] The difference in the MM energy changes of Systems 1 and 3. [e] The estimate of the activation free energy (the entropic and thermal enthalpic contributions are taken from Table 3).

Table 2 The calculated QM/MM reaction energies ($\Delta E_{QM/MM}$) for O–O bond cleavage in MCOs along with the individual contributions[a]

Cu-T2 ligand	Central ligand	Charge of S1	$\Delta E_{QM/vac}$[b]	ΔE_{MM}[c]	$\Delta E_{QM/MM}$	$\Delta G_{QM/MM}$[d]
H_2O	O_2H^-	1	−93.9	−9.8	−58.8	−43.4
OH^-	O_2H^-	0	−135.1	−1.9	−101.4	−88.1
—	O_2H^-	1	−42.1	23.8	−26.4	−8.0
H_2O	O_2^{2-}	0	40.4	−0.6	49.0	51.9
OH^-	O_2^{2-}	-1	−178.2	0.1	−107.2	−78.9
—	O_2^{2-}	0	24.5	3.1	36.6	52.4

[a] The geometries were optimised at the QM(RI-PBE/DZP)/MM level, whereas the single-point energies were recalculated at the QM(B3LYP/def2-TZVP)/MM level. The total energies of the reactants (**NI′**) are set to zero. All of the values are in kJ mol^{-1}. [b] The *in vacuo* QM energy change of System 1. [c] The difference in the MM energy changes of Systems 1 and 3. [d] The estimate of the activation free energy (the entropic and thermal enthalpic contributions are taken from Table 3).

energies of the two species), the QM/MM activation barrier associated with the **NI′**{OH^-,—,O_2H^-} state is estimated to be $\Delta E^{\neq} \approx 59$ kJ mol^{-1} as compared to the $\Delta E^{\neq} \approx 71$–72 kJ mol^{-1} obtained for the **NI′**{H_2O,—,O_2^{2-}} state. Note that other alternatives included in Table 1 also have higher barriers than **NI′**{OH^-,—,O_2H^-}. Moreover, on the product side, **NI**{OH^-,OH^-,O^{2-}:C} is 122 kJ mol^{-1} more stable than **NI**{H_2O,O^{2-},O^{2-}:C}, which is in agreement with the assumed protonation state of the observed NI.[14,17] As can be seen in Table 2, the calculated thermodynamic driving force for the **NI′**{HO^-,—,O_2H^-} → **NI**{OH^-,OH^-,O^{2-}:C} reaction is $\Delta G_{QM/MM} = 88$ kJ mol^{-1} ($\Delta E_{QM/MM} = 101$ kJ mol^{-1}), which lowers the

exothermicity of the reaction by ~120 kJ mol^{-1} when compared to the QM cluster model.[25] This fact demonstrates the role of the enzyme in buffering the excess reaction energy of this highly exothermic reaction.

In conclusion, the QM/MM calculations suggest that the most plausible reaction pathway is the **NI′**{OH^-,—,O_2H^-} → **NI**{OH^-,OH^-,O^{2-}:C}. This reasoning is similar to the discussed high- and low-pK_a pathways reported by Yoon and Solomon in their QM study[25] of O_2 cleavage. However, the QM/MM calculations predict a more important role of the protonation of the peroxide than the QM calculations do (the $\Delta\Delta E_{QM}^{\neq}$ between the pathways with and without a proton was only 0.5 kcal mol^{-1}).[25]

In Table 2, we have collected the calculated reaction energies for the six studied pathways. In contrast to the activation barriers (Table 1), the differences between the reaction energies are much larger, ranging from $\Delta E = -107$ kJ mol^{-1} for the **NI′**{OH^-,—,O_2^{2-}} → **NI**{OH^-,O^{2-},O^{2-}:C} pathway to $\Delta E = +49$ kJ mol^{-1} for the **NI′**{H_2O,—,O_2^{2-}} → **NI**{H_2O,O^{2-},O^{2-}:C} pathway. An analysis of the effects that cause these significant differences in the reaction energies is not straightforward. However, some differences can be inferred from the geometrical parameters of the active site depicted in Fig. 5. While geometries of the reactants (**NI′**) and the corresponding TSs are similar, product geometries (**NI**) vary more significantly (*e.g.* the $H_2O\cdots$Cu-T2 distance is 2.32 Å in NI{H_2O,OH^-,O^{2-}:C} *vs.* 3.76 Å in NI{H_2O,O^{2-},O^{2-}:C}). We admit though that this difference in the Cu–O bond itself cannot explain the 156 kJ mol^{-1} difference between the two structures and that also other effects are involved. One might hypothesise that a proper sampling of the conformational space by molecular dynamics or Monte Carlo statistics could partially reduce such large differences in the reaction energies, but it is necessary to add in defence of the static QM/MM approach that many different initial QM/MM structures tend to converge to similar conformations. If there are larger conformational differences (deduced from the $\Delta(E_{MM123}–E_{MM1})$ term), they are usually compensated for by other contributions (see Table S1†).

3.2 Cluster model: entropy contributions

In this study, we have addressed the reactivity of different states of the **NI′** intermediate and attempted to elucidate the most favoured pathway. Since the differences in the TS barriers between the pathways are relatively small, one has to consider also the entropic and thermal enthalpic (further denoted ΔH_{therm}) contributions that need to be added to electronic energies in order to obtain the estimated Gibbs free energies. The entropic term is very sensitive to low-frequency modes in the vibrational partition function and therefore to the proper description of the geometry of the structure (*i.e.* the local minima and first-order saddle points on the potential-energy surfaces must be exactly defined within the approximation), which is problematic in the case of our ComQum QM/MM scheme. Therefore, we used small *in vacuo* QM models of the active site (see the methodological section) to estimate the entropy and thermal enthalpy changes ($\Delta H_{therm} - T\Delta S$) in the protein. We believe such a simplification is reasonable, since large conformational changes are not assumed to occur in the protein except for the active site. This assumption can be supported by the fact that the steric MM energy changes are mostly within 10 kJ mol^{-1}.

In Table 3, the $\Delta H_{therm}^{\neq} - T\Delta S^{\neq}$ and $\Delta H_{therm} - T\Delta S$ terms contributing to the activation barrier and reaction energies are provided. In both cases, their values are similar for all six of the alternative pathways. The effect of $\Delta H_{therm}^{\neq} - T\Delta S^{\neq}$ on the barriers is relatively small (from −3 kJ mol^{-1} to 5 kJ mol^{-1}), implying that the essential chemistry of the O_2 cleavage in MCOs is reasonably well predicted already by the values of $\Delta E^{\neq}$. Comparing the entropic and enthalpic contributions (the most dominant vibrational terms are shown in Table S2†), it appears that both of them are of a similar magnitude (the entropy term is slightly greater) but of the opposite sign. In

Table 3 The calculated gas-phase activation energies ($\Delta E_{QM}^{\neq}$) and reaction energies (ΔE_{QM}), along with an estimation of the thermal enthalpic and entropic contributions ($\Delta H_{therm}^{(\neq)} - T\Delta S^{(\neq)}$) to the reaction or activation free energies ($\Delta G^{(\neq)}_{QM}$) are displayed[a]

Cu-T2 ligand	Central ligand	Charge of QM clust.	$\Delta E^{\neq}_{QM}$	$\Delta H^{\neq}_{therm} - T\Delta S^{\neq}$	$\Delta G^{\neq}_{QM}$	ΔE_{QM}	$\Delta H_{therm} - T\Delta S$	ΔG_{QM}
H_2O	O_2H^-	3	50.4	−2.5	47.9	−113.6	15.4	−98.3
OH^-	O_2H^-	2	—	—	—	−141.7	13.3	−128.4
—	O_2H^-	3	33.4	−1.2	32.2	−118.5	18.4	−100.1
H_2O	O_2^{2-}	2	39.7	1.3	41.0	−41.7	12.9	−28.8
OH^-	O_2^{2-}	1	79.4	5.6	85.0	−95.9	22.8	−73.1
—	O_2^{2-}	2	39.8	4.5	44.3	−42.7	15.8	−26.9

[a] The results were obtained at the B3LYP/def2-TZVP//RI-PBE/DZP level, whereas the thermochemical analysis ($\Delta H_{therm} - T\Delta S$ term) was carried out at the RI-PBE/DZP level. The total energies of the reactants (NI′) are set to zero. All of the values are in kJ mol^{-1}.

spite of our extensive efforts, we did not succeed in an optimisation of the TS of the *in vacuo* QM model corresponding to the **NI′**{OH^-,—,O_2H^-} → **NI**{OH^-,OH^-,O^{2-}:C} pathway. However, the rather small scattering of the calculated $\Delta H_{therm}^{\neq} - T\Delta S^{\neq}$ values obtained for the other systems (pathways) gives us an ample amount of confidence that the activation entropic and enthalpic changes in this favoured pathway will be similar, namely $\Delta G_{QM/MM}^{\neq} \approx$ 60–65 kJ mol^{-1}.

The $\Delta H_{therm} - T\Delta S$ contributions to the reaction energies range from 13 kJ mol^{-1} to 23 kJ mol^{-1}. The results of the analysis displayed in Table S2† show that $-T\Delta S$ (*i.e.* $-T\Delta S_{vib}$) is the dominant term. It implies that the **NI** structures are entropically disfavoured as compared to the corresponding **NI′** intermediates (by approximately 15 kJ mol^{-1}).

It is also interesting to compare the energetics of the reaction obtained for the QM clusters and QM/MM models of the enzyme. The barriers are significantly lower in the majority of QM models with respect to the QM/MM calculations (*e.g.* 33 kJ mol^{-1} *vs.* 73–79 kJ mol^{-1} for the **NI′**{—,—,O_2H^-} → **NI**{—,OH^-,O^{2-}:C} pathway). As for the reaction energies, the general trend is in accordance with the previous discussion: the NI products are significantly more stable in reference to the **NI′** reactants using the gas-phase QM models when compared to the corresponding QM/MM models. It is in agreement with the above-mentioned Hammond's postulate and our previous observations:[24] the overstabilisation of the product state leads to an artificial lowering of the activation barrier (as depicted in Fig. 2). Finally, it can be also mentioned that the solvation effect represented by an implicit solvent model (COSMO)[48] with a permittivity of 4 or 20 is rather small (*cf.* Table S3†). Therefore, we may conclude that the explicit inclusion of the whole protein and solvent water molecules by means of a QM/MM scheme leads to significantly improved energies.

3.3 The multireference CASSCF/CASPT2 calculations

The accuracy of the CASSCF/CASPT2 method applied to reactions with a large change in the molecular electronic structure, *i.e.* processes in which bonds are broken and/or formed, strongly depends on the selected active space. In an optimal case, a full-valence active space should be sufficient for an accurate prediction of the energetics of a reaction. Unfortunately, such an active space is too large to be computationally manageable for even a minimalistic model of bioinorganic complexes (*e.g.* an active site of metalloenzymes). In this study, we attempted to estimate the activation barriers and reaction energies of the gas-phase models of the

studied **NI′** → **NI** reaction at the CASSCF/CASPT2 level. As mentioned in the Computational Details section, we considered the distribution of fifteen electrons in nine MOs: six in the O_2 moiety (*i.e.* σ, 2π, 2π*, σ*) along with $3d_{Cu}$ orbitals as an adequate (minimal) active space. We may present, at the moment, the first value obtained for the **NI′**{H_2O,—,O_2^{2-}} → **NI**{H_2O,O^{2-},O^{2-}:C} pathway although it was achieved using a smaller (15-in-9) active space. The CASSCF/CASPT2 activation barrier has been calculated to be $\Delta E_{QM}^{\neq} = 45$ kJ mol^{-1}, which is in very good agreement with the value of 40 kJ mol^{-1} reported in Table 3 for this pathway. A full set of CASSCF(15-in-9)/CASPT2 values would be, however, necessary to make conclusive observations.

4 Conclusions

In the current study, we investigated the reductive cleavage of the O–O bond by MCOs in detail using the QM/MM method and compared the calculated data with their counterparts obtained using the cluster model (QM). We have shown that the most favourable pathway involves a protonation of the peroxide moiety within the TNC and its subsequent cleavage. The calculated activation barriers are in good agreement with the experimental barrier, and it has been shown that only by including the whole protein (*via* the QM/MM approach) were we able to buffer the large exothermicity of the reaction. We have also demonstrated that the entropic and thermal enthalpy corrections do not play a crucial role in distinguishing between the studied pathways although they correct the calculated barriers by 5–20 kJ mol^{-1} on an absolute scale. Finally, an attempt is presented to carry out the CASSCF/CASPT2 calculations for the studied reaction in order to validate the (in principle single-determinantal) DFT method used, and the preliminary results show a reasonable agreement between the two methods.

Acknowledgements

We gratefully acknowledge financial support from the Ministry of Education, Youth and Sports of the Czech Republic (Research Projects Z40550506 and LC512) and from the Swedish Research Council (UR).

References

1 H. M. Senn and W. Thiel, *Angew. Chem., Int. Ed.*, 2009, **48**, 1198–1229.
2 S. C. L. Kamerlin, M. Haranczyk and A. Warshel, *J. Phys. Chem. B*, 2009, **113**, 1253–1272.
3 P. E. M. Siegbahn and F. Himo, *JBIC, J. Biol. Inorg. Chem.*, 2009, **14**, 643–651.
4 H. Hu and W. T. Yang, *Annu. Rev. Phys. Chem.*, 2008, **59**, 573–601.
5 U. Ryde, *Curr. Opin. Chem. Biol.*, 2003, **7**, 136–142.
6 B. Kirchner, F. Wennmohs, S. F. Ye and F. Neese, *Curr. Opin. Chem. Biol.*, 2007, **11**, 134–141.
7 F. Neese, *Coord. Chem. Rev.*, 2009, **253**, 526–563.
8 A. Warshel, *Computer Modeling of Chemical Reactions in Enzymes and Solutions*, John Wiley & Sons, Inc., New York, 1997.
9 L. Hu, J. Eliasson, J. Heimdal and U. Ryde, *J. Phys. Chem. A*, 2009, **113**, 11793–11800.
10 A. Messerschmidt, in *Multicopper oxidases*, ed. A. Messerschmidt, World Scientific, Singapore; River Edge, NJ, 1997, pp. 23–80.
11 E. I. Solomon, U. M. Sundaram and T. E. Machonkin, *Chem. Rev.*, 1996, **96**, 2563–2605.
12 W. Shin, U. M. Sundaram, J. L. Cole, H. H. Zhang, B. Hedman, K. O. Hodgson and E. I. Solomon, *J. Am. Chem. Soc.*, 1996, **118**, 3202–3215.
13 A. E. Palmer, S.-K. Lee and E. I. Solomon, *J. Am. Chem. Soc.*, 2001, **123**, 6591–6599.
14 S.-K. Lee, S. D. George, W. E. Antholine, B. Hedman, K. O. Hodgson and E. I. Solomon, *J. Am. Chem. Soc.*, 2002, **124**, 6180–6193.
15 K. Piontek, M. Antorini and T. Choinowski, *J. Biol. Chem.*, 2002, **277**, 37663–37669.
16 S. A. Roberts, G. F. Wildner, G. Grass, A. Weichsel, A. Ambrus, C. Rensing and W. R. Montfort, *J. Biol. Chem.*, 2003, **278**, 31958–31963.
17 L. Rulíšek, E. I. Solomon and U. Ryde, *Inorg. Chem.*, 2005, **44**, 5612–5628.

18 F. Xu, *Biochemistry*, 1996, **35**, 7608–7614.
19 G. J. Davies and V. Ducros, in *Handbook of Metalloproteins*, ed. A. Messerschmidt, R. Huber, K. Wieghardt and T. Poulos, Wiley, New York, 2001, pp. 1359–1368.
20 J. Chalupský, F. Neese, E. I. Solomon, U. Ryde and L. Rulíšek, *Inorg. Chem.*, 2006, **45**, 11051–11059.
21 U. Ryde, Y.-W. Hsiao, L. Rulíšek and E. I. Solomon, *J. Am. Chem. Soc.*, 2007, **129**, 726–727.
22 E. I. Solomon, A. J. Augustine and J. Yoon, *Dalton Trans.*, 2008, 3921–3932.
23 J. Yoon, L. M. Mirica, T. D. P. Stack and E. I. Solomon, *J. Am. Chem. Soc.*, 2005, **127**, 13680–13693.
24 M. Lepšík, M. Srnec, D. Hnyk, B. Grüner, J. Plešek, Z. Havlas and L. Rulíšek, *Collect. Czech. Chem. Commun.*, 2009, **74**, 1–27.
25 J. Yoon and E. I. Solomon, *J. Am. Chem. Soc.*, 2007, **129**, 13127–13136.
26 P. W. Atkins, *Physical Chemistry*, Oxford University Press, Oxford, U.K., 1978.
27 G. S. Hammond, *J. Am. Chem. Soc.*, 1955, **77**, 334–338.
28 U. Ryde, *J. Comput.-Aided Mol. Des.*, 1996, **10**, 153–164.
29 U. Ryde and M. H. M. Olsson, *Int. J. Quantum Chem.*, 2001, **81**, 335–347.
30 O. Treutler and R. Ahlrichs, *J. Chem. Phys.*, 1995, **102**, 346–354.
31 D. A. Case, T. A. Darden, T. E. Cheatham III, C. L. Simmerling, J. Wang, R. E. Duke, R. Luo, K. M. Merz, B. Wang, D. A. Pearlman, M. Crowley, S. Brozell, V. Tsui, H. Gohlke, J. Mongan, V. Hornak, G. Cui, P. Beroza, C. Schafmeister, J. W. Caldwell, W. S. Ross and P. A. Kolman, *AMBER 8*, University of California, San Francisco, 2004.
32 W. D. Cornell, P. Cieplak, C. I. Bayly, I. R. Gould, K. M. Merz, D. M. Ferguson, D. C. Spellmeyer, T. Fox, J. W. Caldwell and P. A. Kollman, *J. Am. Chem. Soc.*, 1995, **117**, 5179–5197.
33 S. A. Roberts, A. Weichsel, G. Grass, K. Thakali, J. T. Hazzard, G. Tollin, C. Rensing and W. R. Montfort, *Proc. Natl. Acad. Sci. U. S. A.*, 2002, **99**, 2766–2771.
34 J. P. Perdew, K. Burke and M. Ernzerhof, *Phys. Rev. Lett.*, 1996, **77**, 3865–3868.
35 K. Eichkorn, O. Treutler, H. Öhm, M. Häser and R. Ahlrichs, *Chem. Phys. Lett.*, 1995, **240**, 283–290.
36 K. Eichkorn, F. Weigen, O. Treutler and R. Ahlrichs, *Theor. Chem. Acc.*, 1997, **97**, 119–124.
37 W. J. Hehre, L. Radom, P. v. R. Schleyer and J. A. Pople, *Ab initio molecular orbital theory*, Wiley-Interscience, New York, 1986.
38 A. Schäfer, C. Huber and R. Ahlrichs, *J. Chem. Phys.*, 1994, **100**, 5829–5835.
39 F. Weigend and R. Ahlrichs, *Phys. Chem. Chem. Phys.*, 2005, **7**, 3297–3305.
40 A. D. Becke, *Phys. Rev. A: At., Mol., Opt. Phys.*, 1988, **38**, 3098–3100; C. T. Lee, W. T. Yang and R. G. Parr, *Phys. Rev. B: Condens. Matter*, 1988, **37**, 785–789; A. D. Becke, *J. Chem. Phys.*, 1993, **98**, 5648–5652.
41 F. Jensen, *Introduction to Computational Chemistry*, John Wiley & Sons, 1999.
42 B. O. Roos and P. R. Taylor, *Chem. Phys.*, 1980, **48**, 157–173.
43 K. Andersson, P.-Å. Malmqvist and B. O. Roos, *J. Chem. Phys.*, 1992, **96**, 1218–1226.
44 G. Karlström, R. Lindh, P.-Å. Malmqvist, B. O. Roos, U. Ryde, V. Veryazov, P.-O. Widmark, M. Cossi, B. Schimmelphennig, P. Neogrady and L. Seijo, *Comput. Mater. Sci.*, 2003, **28**, 222–239.
45 B. O. Roos and K. Andersson, *Chem. Phys. Lett.*, 1995, **245**, 215–243; N. Forsberg and P.-Å. Malmqvist, *Chem. Phys. Lett.*, 1997, **274**, 196–204.
46 K. Pierloot, B. Dumez, P.-O. Widmark and B. O. Roos, *Theor. Chim. Acta*, 1995, **90**(2–3), 87–114.
47 A. J. Augustine, L. Quintanar, C. S. Stoj, D. J. Kosman and E. I. Solomon, *J. Am. Chem. Soc.*, 2007, **129**, 13118–13126.
48 A. Klamt and G. Schuurmann, *J. Chem. Soc., Perkin Trans. 2*, 1993, 799–805; A. Schäfer, A. Klamt, D. Sattel, J. C. W. Lohrenz and F. Eckert, *Phys. Chem. Chem. Phys.*, 2000, **2**, 2187–1293.